

Electrical Facility Effects on Hall-Effect-Thruster Cathode Coupling: Discharge Oscillations and Facility Coupling

Jonathan A. Walker,* Jason D. Frieman,† and Mitchell L. R. Walker‡

Georgia Institute of Technology, Atlanta, Georgia 30332

Vadim Khayms§

Lockheed Martin Space Systems Company, Sunnyvale, California 94089

and

David King¶ and Peter Y. Peterson**

Aerojet Rocketdyne, Inc., Redmond, Washington 98052

DOI: 10.2514/1.B35835

The physical mechanisms that govern the electrical interaction between the Hall-effect-thruster electrical circuit and the conductive vacuum-facility walls are not fully understood. As a representative test bed, an Aerojet Rocketdyne T-140 Hall-effect thruster is operated at 3.05 kW and a xenon mass flow rate of 11.6 mg/s with a vacuum facility operating neutral pressure of 7.3×10^{-6} torr, corrected for xenon. Two electrical witness plates, representative of the facility chamber walls, are placed 2.3 m radially outward from thruster centerline and 4.3 m axially downstream from the thruster exit plane. The cathode is radially translated from 18.1 to 77.8 cm away from the thruster centerline. At each cathode position, the discharge current and the electrical waveform of the radial and axial plates are simultaneously measured. As the cathode radial position changes from 18.1 to 77.8 cm from the thruster centerline, the discharge-current oscillation frequency decreases between 17 and 35% for the electrically grounded thruster-body case, and between 15 and 23% for the electrically floating thruster-body case. The analysis of the electron current collected by the radial plate suggests that electrons directly sourced from the cathode impinge on the radial plate at large cathode positions. Overall, the results of this work show that the chamber walls act as an artificial electrical boundary condition that keeps the Hall-effect-thruster plume plasma potential to within certain bounds.

Nomenclature

B	=	magnitude of the magnetic field, T
$\text{cov}(X, Y)$	=	covariance of two signals X and Y
e	=	electron charge, C
m_e	=	mass of electron, kg
$R(X, Y)$	=	correlation coefficient of two signals X and Y
ν	=	electron-neutral collision frequency, s^{-1}
β	=	electron Hall parameter
Ω_e	=	electron gyrofrequency, $rad \cdot s^{-1}$

I. Introduction

TO INCREASE the return on investment of commercial satellites and the science return for exploratory missions, much effort has

been placed into the development and testing of Hall-effect thrusters (HETs). Because of their low thrust, as compared to chemical propulsion, mission requirements often require thruster operational lifetimes on the order of thousands of hours [1–3]. To ensure that the operational lifetime of the HET meets the mission requirements, lifetime qualification tests are performed in ground-based vacuum facilities. The operational time for ground-based lifetime qualification depends on mission requirements; however, qualification tests are typically performed between 5000 and 10,000 h, and represent a major development cost of HETs [1,4]. To ensure a successful on-orbit operation of HETs, the ground-based testing environment must be representative of the on-orbit environment, or there must be a clear path to correlate the ground-test results to expected on-orbit HET behavior.

Efforts to characterize the impact of the vacuum facility on HET operation and plume characteristics have been primarily focused on the effect of facility background neutral pressure on HET performance and plume properties [5–12]. In addition to neutral background-pressure facility effects, a growing body of evidence suggests that the HET interacts electrically with the conductive vacuum chamber [13–15]. The results of this work indicate that the position of the cathode with respect to the centerline of the thruster and the magnetic-field topology greatly impacts the role of the conducting vacuum facility in the HET electrical circuit. Specifically, it was shown that the electron recombination pathways exhibit regional behavior with respect to cathode position [14]. For cathode locations with a much greater-than-unity electron Hall parameter, the magnetization of the electrons due to the HET magnetic field resulted in an increased electron flux to the grounded HET body. This flux to the HET body in a ground-based testing facility represents an ion-electron recombination surface that is not normally present for in-flight HET operation. For cathode locations where the electron Hall parameter approached unity, neutralization electrons were electrostatically drawn into the plume, and were able to preferentially recombine with ions in the plume or via collection by the axially downstream chamber surfaces. For cathode locations where the electron Hall parameter was much less than unity (which correspond to far-field cathode positions), the increased proximity of the cathode

Received 7 April 2015; revision received 2 November 2015; accepted for publication 9 November 2015; published online 11 January 2016. Copyright © 2015 by Jonathan A. Walker, Jason D. Frieman, and Mitchell L.R. Walker. Published by the American Institute of Aeronautics and Astronautics, Inc., with permission. Copies of this paper may be made for personal or internal use, on condition that the copier pay the \$10.00 per-copy fee to the Copyright Clearance Center, Inc., 222 Rosewood Drive, Danvers, MA 01923; include the code 1533-3876/15 and \$10.00 in correspondence with the CCC.

*Graduate Research Assistant, Aerospace Engineering, High-Power Electric Propulsion Laboratory; jwalker30@gatech.edu. Student Member AIAA.

†Graduate Research Assistant, Aerospace Engineering, High-Power Electric Propulsion Laboratory; jfrieman3@gatech.edu. Student Member AIAA.

‡Associate Professor, Aerospace Engineering, High-Power Electric Propulsion Laboratory; mitchell.walker@ae.gatech.edu. Associate Fellow AIAA.

§Electric Propulsion Architect; vadim.khayms@lmco.com. Senior Member AIAA.

¶Technical Fellow, Engineering; david.king@rocket.com. Senior Member AIAA.

**Project Engineering Specialist, Engineering; peter.peterson@rocket.com. Senior Member AIAA.

to the radial walls of the vacuum-chamber facility caused the radial facility surfaces to occupy a significant percentage of the cathode-plume solid angle, and thus, caused the emergence of an electron-ion recombination pathway through the radial facility surfaces to ground. Despite the observed changes in electron pathways, measurements of the plume properties and thruster performance showed no discernable changes as a function of cathode position with respect to thruster centerline [14].

The aforementioned previous work examined the electron-ion recombination pathways and HET behavior from a time-averaged analysis. The HET discharge plasma, however, is a dynamic system, resulting in fundamental plasma oscillatory modes that are not directly observable from time-averaged measurements [16–28]. The oscillatory plasma modes' types, frequencies, and spectral powers present in the discharge can impact HET stability and performance [20]. Because previous work on electrical facility effects has not delved into the analysis of time-dependent properties of the HET discharge, such as breathing-mode frequency and peak-to-peak discharge current, it may be the case that altering the electron-ion recombination pathways affects the HET time-dependent behavior. Furthermore, the previous work demonstrated the dependence of the electron recombination pathways on cathode position with respect to thruster centerline, but was only able to posit the source of electrons recombining on the radial plate.

The goal of this work was to determine the influence of the cathode position on the time-resolved behavior of the HET discharge, and to understand the physical mechanisms driving the electron flux measured on the representative chamber surfaces presented in Frieman et al. [14] through the use of temporally resolved waveform analysis. By using simultaneous current-waveform measurements of the HET and current- and voltage-waveform measurements of the chamber plates, this work will examine how the HET thruster time-dependent behavior responds to changes in cathode position. The HET is the dominant plasma source in the chamber, and should mediate the measured electron current on the radial chamber surface. The statistical correlation of the time-resolved voltage and current waveforms of the chamber plates and discharge current will provide quantifiable measurements of electrical connection between the HET and the surrounding facility. Further understanding of the physical mechanisms governing the HET electrical interaction is gained by comparing power-spectrum peaks between the aforementioned current and voltage electrical waveforms. Specifically, this work focuses on the coupling of the HET discharge current to the radial chamber surface, and through the use of time-resolved analysis, is able to support previous conclusions drawn from prior work's analysis of time-averaged plume measurements, and provide new insight into the physical connection between the HET and the radial chamber surface.

II. Experimental Apparatus

A. Vacuum Facility

All experiments were performed in the Vacuum Test Facility 2 (VTF-2) at the Georgia Institute of Technology High-Power Electric Propulsion Laboratory. Figure 1 shows a schematic of this facility. The VTF-2 is a stainless-steel chamber measuring 9.2 m in length and 4.9 m in diameter. It is evacuated to rough vacuum using one 495 CFM rotary-vane pump and one 3800 CFM blower. High vacuum is achieved using 10 CVI TMI reentrant cryopumps that have a liquid nitrogen cooled shroud and a helium cold-gas cycle cooled pumping surface. The cryopump shrouds are fed using the Stirling Cryogenics SPC-8 RL special closed-loop nitrogen-liquefaction system detailed by Kieckhafer and Walker [29]. The facility has a combined nominal pumping speed of 350,000 L/s on xenon, and can achieve a base pressure of 1.9×10^{-9} torr. Pressure in the VTF-2 was monitored using two Agilent BA 571 hot-filament ionization gauges controlled by an Agilent XGS-600 Gauge Controller. The pressure-measurement uncertainty of the Agilent BA 571 is expected to be +20, -10% of indicated pressure [30]. One gauge was mounted to a flange on the exterior of the chamber, whereas the other was mounted 0.6 m radially outward from the thruster centered on the exit plane. To

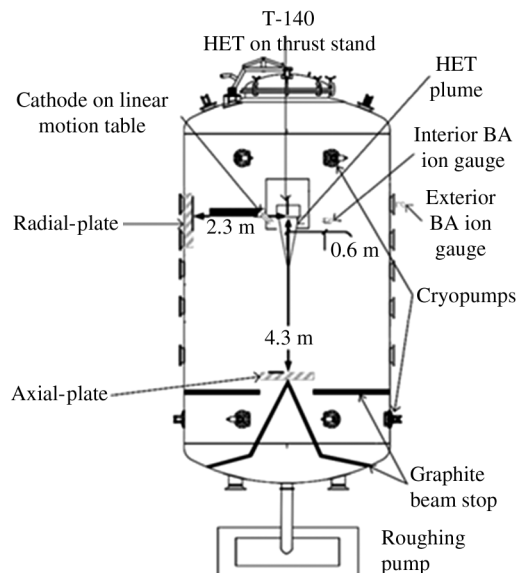


Fig. 1 Facility overview of experimental apparatus; diagram is not to scale. BA ion gauge refers to an Agilent Bayard-Alpert (BA) 571 hot-filament ion gauge.

prevent plume ions from having a direct line of sight to the ionization-gauge filament of the interior ion gauge and potentially affecting the pressure measurement, a neutralizer identical to the one used by Walker and Gallimore [31] was attached to the gauge orifice. The nominal operating pressure for this work, as measured by the interior and exterior ion gauges, was 1.3×10^{-5} and 7.3×10^{-6} torr corrected for xenon, respectively. As specified by the manufacturer, the corrected pressure P_c is found by relating the indicated pressure P_i and the vacuum-chamber base pressure P_b to a gas-specific constant using the following equation [32]:

$$P_c = \frac{P_i - P_b}{2.87} + P_b \quad (1)$$

B. T-140 HET and EPL 500 Cathode

All experiments detailed in this work were performed using the Aerojet Rocketdyne T-140 HET originally developed by Space Power, Inc. in collaboration with the Keldysh Research Center and Matra Marconi Space [33]. The T-140 HET is a laboratory-model HET that has a discharge channel made of M26-grade boron nitride with an outer diameter of 143 mm. The performance of the T-140 has been extensively mapped by prior investigations [33]. The thruster body was isolated from facility ground, such that the thruster body can be electrically configured as either floating or grounded.

High-purity (99.9995%) xenon propellant was supplied to the thruster and cathode using stainless-steel lines metered with MKS 1179A mass flow controllers. The controllers were calibrated before each test by measuring gas pressure and temperature as a function of time in a known control volume. After calibration, the mass flow controllers have an uncertainty of ± 0.03 mg/s (5.1%) for the cathode flow and ± 0.12 mg/s (2%) for the anode flow.

An Electric Propulsion Laboratory Hollow Cathode Plasma Electron Emitter 500 series cathode was located at the 9 o'clock position of the thruster. The cathode flow rate was set to a constant 1.16 mg/s for all thruster operating conditions. The orifice location of the cathode was located approximately 2.5 cm downstream of the thruster exit plane at a fixed declination of 55 deg with respect to the thruster centerline. The nominal radial position of the cathode was 18.1 cm outward from the thruster centerline. Time-resolved measurements of the discharge current, radial-chamber-plate current and voltage, and axial-chamber-plate current and voltage were taken for the radial positions of the cathode orifice from 18.1 to 77.8 cm

Table 1 Approximate magnetic-field strength as a function of cathode-orifice radial location away from thruster centerline

Radial location, cm	Magnetic-field strength, G
18.1	30
19.4	20
20.9	20
39.0	10
47.5	0

outward from the thruster centerline using a Parker Daedal 406XR precision linear motion stage with a 2000 mm travel. The positional uncertainty of the motion stage is $\pm 159 \mu\text{m}$. Table 1 shows the computed strength of the magnetic field at the cathode orifice as a function of radial location away from the thruster centerline. The magnetic-field topology listed in Table 1 is calculated using a two-dimensional Infolytica MagNet model of the T-140 HET magnetic circuit.

The magnetic-circuit configuration of the T-140 HET (two concentric coils centered on the thruster centerline) restricts the position of the magnetic-field separatrix to the thruster centerline, and precludes the T-140 HET from exhibiting the off-centerline separatrix surfaces shown in HETs with magnetic coils placed off thruster centerline [34–36]. This magnetic-field topology eliminates any concerns about the changing nature of the near-field plume properties and cathode coupling as a function of cathode position relative to the absent off-centerline separatrix surface [34–36].

All data were collected with the T-140 HET operating at a discharge voltage of 300 V, discharge power of 3.16 kW, an anode xenon flow rate of $11.6 \pm 0.03 \text{ mg/s}$, and a cathode xenon flow rate of $1.61 \pm 0.12 \text{ mg/s}$. The thruster-discharge voltage, inner and outer magnet currents, anode mass flow rate, and cathode mass flow rate were held constant for all test configurations. The thruster was run through a 3 h conditioning cycle prior to data collection to allow the thruster to approach thermal equilibrium [33].

The T-140 HET discharge was controlled using a Magna-Power TSA800-54 power supply. The thruster inner and outer magnet coils were powered with TDK-Lambda GEN60-25 power supplies. A TDK-Lambda Genesys 150 V/10 A and a TDK-Lambda Genesys 40 V/38 A power supply were used to power the cathode keeper and heater, respectively. The thruster-discharge supply was connected to a discharge filter consisting of a $95 \mu\text{F}$ capacitor and 1.3Ω resistor to prevent oscillations over 1.4 kHz in the discharge current from reaching the discharge supply. Diagnostic and power connections entered the VTF-2 through separate feedthroughs on separate flanges to eliminate potential cross talk between the thruster-discharge power lines and diagnostic lines. Figure 2 shows the circuit used to operate the T-140 HET in this work.

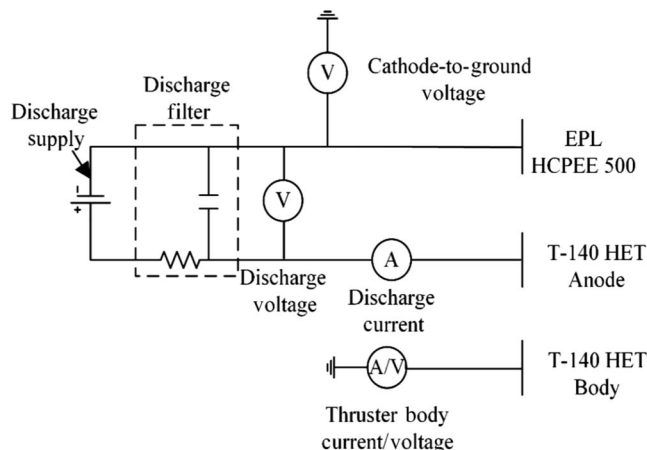


Fig. 2 Electrical diagram of current and voltage measurements of the HET discharge circuit.

The discharge-current oscillations, measured at the thruster side of the discharge filter, of the T-140 HET were recorded using a Teledyne LeCroy CP150 current probe connected to a Teledyne LeCroy HDO6104 oscilloscope. The uncertainty and bandwidth of the current probe are $\pm 1\%$ and 10 MHz; for the oscilloscope, they are $\pm 0.5\%$ full scale and 1 GHz. In the floating thruster-body configuration, the thruster-body floating voltage was measured differentially using Teledyne LeCroy PP018 passive probes with a bandwidth of 500 MHz and an accuracy of $\pm 0.5\%$ connected to the Teledyne LeCroy oscilloscope. When the thruster body was grounded, the current conducted through the thruster body to ground was measured using a Teledyne LeCroy CP030 current probe connected to the Teledyne LeCroy oscilloscope. The CP030 has a bandwidth of 50 MHz and an accuracy of $\pm 1\%$. A filter sensitivity analysis of the discharge-current filter operating in tandem with the discharge supply and hall thruster, as described by Spektor et al. [37], was not performed.

The mean discharge voltage of the T-140 HET was measured differentially using a pair of Teledyne LeCroy PPE 2 kV 100:1 high-voltage probes connected to a Tektronix TDS3034B oscilloscope. The bandwidth of the voltage probes is 400 MHz; the oscilloscope has an uncertainty and bandwidth of $\pm 2\%$ and 300 MHz. The cathode-to-ground voltage was measured differentially using two Tektronix P6139A passive probes connected to the Tektronix oscilloscope, which have a bandwidth of 500 MHz and an accuracy of $\pm 0.5\%$. This was done to ensure that the HET electrical circuit remained floating relative to ground. Figure 2 shows the location of each telemetry measurement in the T-140 HET circuit.

C. Configuration of Plates

To assess the impact of the conductive walls of the vacuum-chamber facility on HET operation, two $0.91 \text{ m} \times 0.91 \text{ m} \times 0.16 \text{ cm}$ thick square aluminum plates serve as representative chamber surfaces. Each plate was mounted adjacent to, but electrically isolated from, the walls of the vacuum test facility. One plate is placed 4.3 m downstream from the exit plane of the thruster, and is referred to as the “axial chamber plate” or “axial plate.” The other plate was located 2.3 m radially outward from the thruster centerline and centered on the exit plane of the T-140 HET, and is referred to as the “radial chamber plate” or “radial plate.” These two locations were chosen, as each location is representative of a unique plasma environment. The axial plate is in a quasi-neutral plasma environment composed primarily of accelerated HET ions and electrons, and the radial plate is in a quasi-neutral plasma environment primarily composed of charge-exchange (CEX) ions and electrons. Figure 1 shows the physical location of the plates with respect to the T-140 HET. Identical plates have been used in previous studies of electrical facility effects [13–15]. Figure 3 shows each of the three plate electrical configurations used in this test. In all three cases, the electrical connection to the plates was made using an RG-58 coaxial cable with a grounded shield that passed through a bayonet Neill-Concelman (BNC) connector feedthrough into the chamber. Based on current measurements made by Frieman et al. [13,14], the current capacity of the inner conductor is sufficient and would not pose any thermal issues on thruster testing. For grounded chamber-plate configurations, grounding occurred in a star-type distribution, as shown in Fig. 3, to the walls of the VTF-2. To prevent ground loops in voltage measurements, the oscilloscope was also grounded to the walls of the VTF-2. For current measurements, ground loops were not a concern, as the current probes are active clamp current monitors.

In configuration A (grounded), each plate was directly connected to chamber ground with the current conducted between each plate and ground measured with a Teledyne LeCroy CP030 current sensor connected to a Teledyne LeCroy HDO6104 oscilloscope; the plate currents and thruster-telemetry waveforms were measured simultaneously at a sampling frequency of 125 MS/s for a 20 ms window to ensure that multiple fundamental discharge-current mode periods were captured. In configuration B (floating), the plates were electrically isolated, and the floating voltage was measured directly using a Teledyne LeCroy PP018 passive probe to the Teledyne

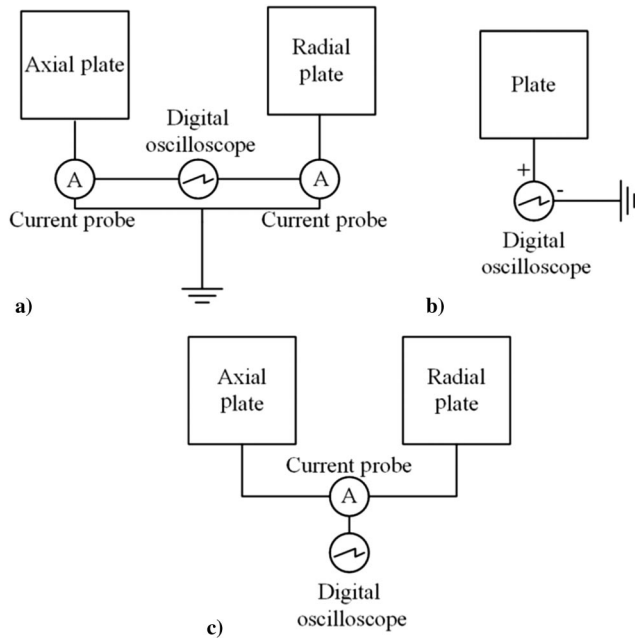


Fig. 3 Plate circuit configurations: a) grounded, b) floating, and c) connected.

LeCroy oscilloscope; these voltage measurements were also taken simultaneously with measurements of the T-140 HET discharge-current oscillations at a sampling frequency of 125 MS/s. In configurations A and B, both plates were simultaneously grounded or floated, respectively. In configuration C (connected), the plates were connected to each other instead of to ground, and the current conducted between the two plates was measured with a Teledyne LeCroy CP030 current probe connected to the Teledyne LeCroy oscilloscope; the current conducted between the two plates and the discharge current were measured simultaneously at a sampling frequency of 125 MS/s.

III. Results

The following sections detail the time-resolved current and voltage measurements on the chamber plates, and the discharge current in both thruster-body electrical configurations as a function of cathode radial distance. The chamber-plate waveform data are measured as a current signal for the grounded and connected configurations, and as a voltage signal for the floating electrical configurations. To understand the nature of the conducting path between the thruster and the wall, each complete set of simultaneous waveform measurements taken from the chamber plates and the discharge current is compared in both the time domain and the frequency domain.

To more clearly discuss the HET and chamber-plate behavior observed at various cathode locations, the discussion of the data presented in the following is divided into regions based on the electron Hall parameter. The electron Hall parameter is defined as the ratio of the electron cyclotron frequency to the electron-neutral collision frequency. In general, the Hall parameter is a way to quantify the magnetization of charged particles by comparing the tendency of the motion of the particle to be dominated by the magnetic field or through collisions with other particles. The Hall parameter can be calculated, as shown in the following equation:

$$\beta = \frac{\Omega_e}{\nu} = \frac{eB}{m_e \nu} \quad (2)$$

in which β is the electron Hall parameter, Ω_e is the electron gyrofrequency, ν is the electron-neutral collision frequency, e is the elementary charge, B is the magnetic-field strength, and m_e is the mass of the electron. An electron Hall parameter of much greater than unity implies that the electrons are magnetized, that is, the electrons are able to complete many orbits around their guiding center before

colliding with a neutral particle. In such a condition, the electron motion is confined by the magnetic-field lines, and they traverse along these magnetic-field lines. An electron Hall parameter much less than unity implies that the electrons are no longer magnetized, that is, the electrons encounter neutral and/or ion collisions before being able to complete one orbit around their guiding center. In such a condition, the electron motion is no longer confined by magnetic-field lines. This approach was used by Frieman et al. [14], and was able to segment the time-averaged data into regions of distinct behavior. The electron Hall parameter at the cathode-orifice estimation as a function of cathode position is more thoroughly covered in Frieman et al. [14]. The results of those regional demarcations based on electron Hall parameter are summarized here. It is important to note that the exact regional delineation based on electron Hall parameter is approximate, and there are transitional Hall parameters between electrons being magnetized and not magnetized. To help with the discussion, these regional positions listed in this work are demarcated by known positions of the cathode at which data were taken. Cathode positions from 18 to 22 cm from the thruster centerline correspond to a region where the electron Hall parameter is much greater than unity. Electrons sourced from the cathode within this spatial region are confined to the magnetic-field lines generated by the HET magnetic coils. These cathode locations are referred to as “region 1.” Cathode positions from 24 to 44 cm from the thruster centerline correspond to a region where the electron Hall parameter is of order unity. Electrons sourced from the cathode are only weakly magnetized, electron Hall parameter of order unity, by the HET magnetic circuit. These cathode locations are referred to as “region 2.” Cathode positions from 47 to 78 cm from the centerline correspond to a region where the electron Hall parameter is much less than unity. The thermal energy of the electrons sourced from the cathode allows them to propagate outward. These cathode locations are referred to as “region 3.” In the following data figures shown, these regions are demarcated by a dashed line overlay. Because of the approximate nature of the regional divisions, there are cathode positions between labeled regions.

A. Thruster-Body Electrical Configuration

In this work, time-resolved waveform measurements were taken when the thruster body of the HET was electrically grounded and when the HET was electrically floating. Because it is typically common for the HET to be tested with the thruster body electrically grounded, as demonstrated by Hofer and Anderson [38], and prior time-averaged measurements of Frieman et al. [14] demonstrated the HET body collects a significant electron current during operation, this investigation’s data collection focused on measuring time-resolved electrical changes for the thruster-body floating configuration. As a result, data collection occurred at more cathode locations with the thruster body electrically floating than the thruster body electrically grounded. To serve as a baseline of comparison, data collection for the thruster body electrically grounded occurred at fewer cathode positions, but with at least one data point in each of the aforementioned regions. By having at least one data point in each cathode-position region, trends drawn from analysis of the floating thruster electrical configuration can be compared against the data points taken for the grounded thruster-body electrical configuration.

B. Discharge Current

To reduce the discharge-current oscillation variability, the discharge-current-waveform data presented for all cases were collected within a 4 h period, without turning off the thruster. In Frieman et al. [14], the mean value of the discharge current did not vary significantly with changes in cathode radial position. However, a time-resolved analysis of the discharge current indicates that other waveform properties do show a dependence on cathode position. As displayed in Fig. 4, the peak to peak of the discharge current, measured as the difference between the maximum current measured and the minimum raw (without filtering) current data measured during an oscilloscope-waveform capture period, has a non-monotonic dependence on cathode radial position. The legend labels

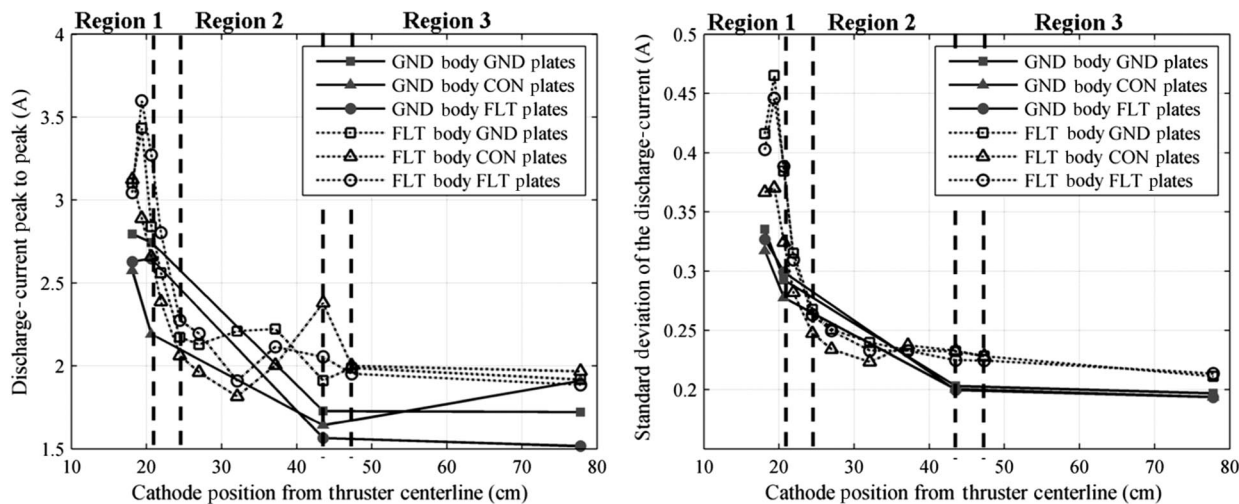


Fig. 4 Peak-to-peak discharge current as a function of cathode-radial-distance (left); standard deviation of the discharge current as a function of cathode-radial-distance (right). Mean discharge current for each data point is 10.2 A with a variability of ± 0.1 A.

in Fig. 4 and all subsequent figures abbreviated the plate and thruster-body electrical configurations as the following: GND represents a grounded electrical configuration, FLT represents a floating electrical configuration, and CON represents a connected electrical configuration. As the cathode moves from region 1 to region 3, the peak-to-peak discharge current drops to approximately 55% of its maximum value for the floating thruster-body configurations, and to 65% of its maximum value for the grounded thruster-body configuration. The peak-to-peak discharge current for the floating thruster-body configuration is 13–18% larger than comparable grounded thruster-body conditions throughout all cathode positions. From region 1 to region 2 cathode positions, the floating thruster-body configuration peak to peak of the discharge current is 60% greater than the grounded thruster-body configuration. From region 2 to region 3 cathode positions, the difference between the floating and grounded thruster-body configurations drops to less than 30%. Because the sampling time of the waveforms is 20 ms, which is hundreds of fundamental breathing-mode cycles, it is possible that the peak-to-peak discharge current is not representative of the actual large-scale changes in discharge-current variability. To verify that the peak-to-peak discharge-current behavior is showing behavior that is representative of aggregate changes in the discharge-current variability, the standard deviation of the discharge current as a function of cathode position is shown in Fig. 4. Because the standard deviation is a statistical quantity that takes into account the variability of the current over the entire sampling window, it is expected that the standard deviation of the discharge current would show smaller overall magnitudes of changes in the discharge current. However, the relative changes in discharge-current standard deviation show a similar cathode-position-dependent behavior as the peak-to-peak discharge current.

For all plate and thruster configurations, the peak-to-peak discharge-current magnitude is dependent on cathode radial position. Because the peak-to-peak discharge-current behavior is indicative of time-dependent processes, it is expected that there is a frequency-domain-dependent behavior as well. Application of a fast Fourier transform (FFT) to a waveform taken in the time domain results in the waveform being resolved in the frequency domain; the square of each amplitude term in the series is known as the power spectrum. The power spectrum shows the distribution of power among the various fundamental frequency modes of a given signal. To obtain only the alternating-current portion of the signal, the time-averaged mean from each waveform was subtracted from the raw waveform. An FFT was applied to that subtracted signal post-thruster testing using MATLAB. To aid in the presentation of the power-spectrum data, the calculated spectral power is converted to units of decibels, as described by Eq. (3):

$$P_{dB} = 10 \log_{10} \frac{P_{calc}}{P_{min}} \quad (3)$$

P_{dB} is the spectral power in units of decibels, P_{calc} is the spectral power in arbitrary units as calculated via the application of the FFT, and P_{min} is the minimum spectral power of the waveform in arbitrary units as calculated via the application of the FFT. The Nyquist–Shannon frequency for current measurements is hardware limited with the discharge-current power spectra being able to resolve frequencies up to 10 MHz, and the chamber-plate current power spectra being able to resolve frequencies up to 30 MHz. The Nyquist–Shannon frequency for floating-voltage measurements is sample rate limited at 62.5 MHz. Based on the sampling size of each waveform, the spectral resolution is 12 Hz. Based on the sampling-time length, the Rayleigh frequency or minimum frequency resolvable is 50 Hz for each power spectrum.

The application of an FFT to the taken discharge-current waveform reveals that the fundamental mode of the discharge-current waveform has a nonmonotonic dependence on cathode position, as shown in Fig. 5. A representative power spectrum of the discharge current is shown in Fig. 6. The peak discharge-current oscillation corresponds to the HET discharge-current breathing mode [16,20,22]. Although there are other fundamental plasma instabilities that occur in the discharge, these modes are not readily identifiable in the measured discharge-current power-spectrum decomposition [16].

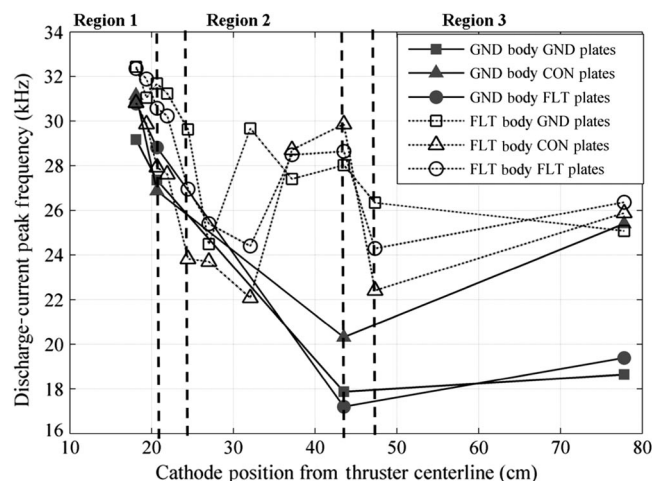


Fig. 5 Peak frequency of the discharge-current power spectra as function of cathode position for the thruster-body and plate electrical configurations.

The discharge-current peak frequency has an overall inverse proportional dependence on cathode position. From region 1 to region 3, the discharge-current peak frequency drops by 15–23% (depending on the plate configuration) for the floating thruster-body

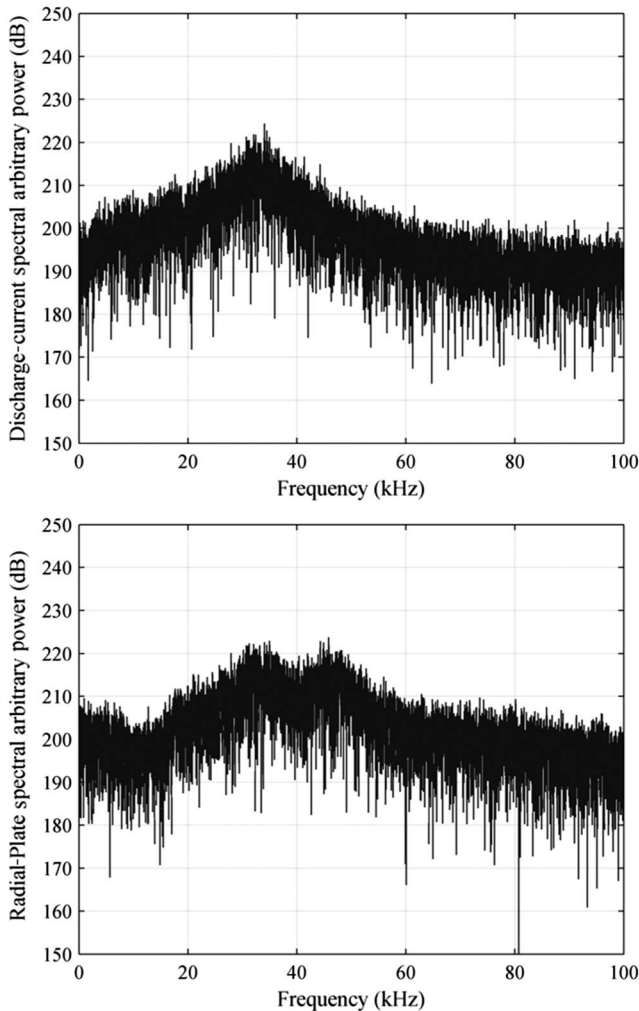


Fig. 6 Power spectra of the discharge current (top); power spectra of the radial-plate current (bottom); waveforms measured for a floating thruster-body and grounded radial-plate configurations at a cathode position of 18.1 cm relative to thruster centerline.

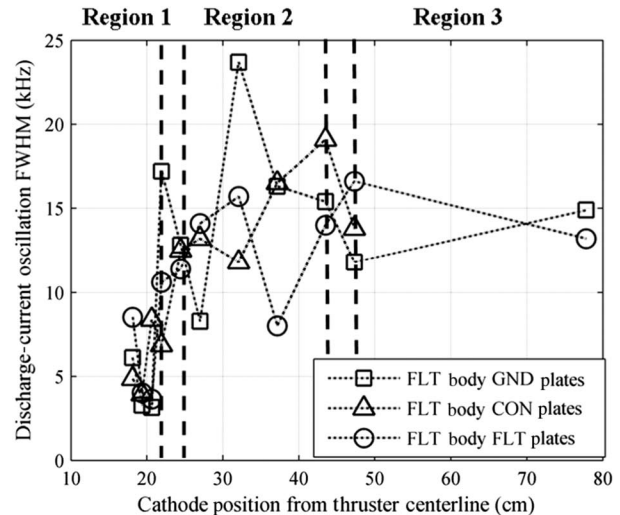
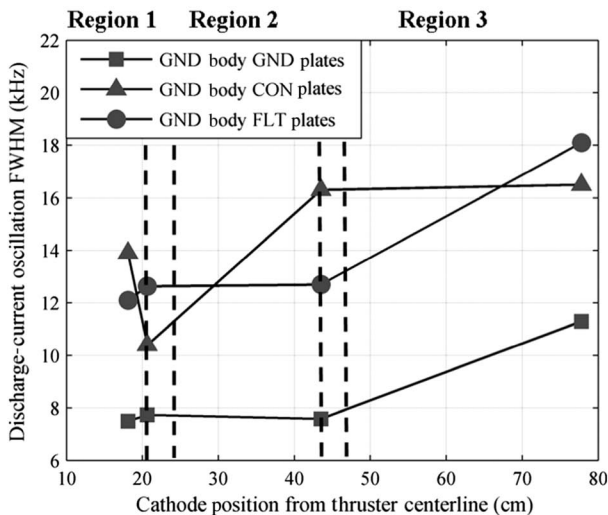


Fig. 7 FWHM of the peak frequency of the power spectrum as a function of cathode radial distance for the electrically grounded thruster-body configuration (left); FWHM of the peak frequency of the power spectrum as a function of cathode radial distance for the electrically floating thruster-body configuration (right).

configuration, and by 17–35% for the grounded thruster-body configuration. In region 1, both the grounded thruster-body and floating thruster-body discharge-current frequency peak show a decrease of approximately 13 and 11%, respectively. In region 2, the grounded thruster-body discharge-current frequency continues to drop to 45% of its 18.1 cm cathode-position value. As compared to the grounded thruster body, the floating thruster-body configuration exhibits a different behavior: in region 2, specifically 30–42 cm, the peak discharge-current oscillation increases to approximately 92% of its region 1 value of 32 kHz.

The discharge-current peak frequency is only indicative of the dominant mode of the HET discharge and does not capture the unsteadiness of the physical plasma process occurring in the HET discharge. The full-width half-maximum (FWHM) is a way to measure such unsteadiness in a time-resolved signal. If the FWHM grows in size, then the thruster begins operating over a larger range of frequencies, thus, meaning, the HET discharge is operating over a larger range of frequencies. The FWHM is determined by measuring the bandwidth between a 3 dB drop or 50% decrease in power from the peak associated with discharge-current oscillation. Figure 7 shows the FWHM of the discharge-current oscillation peak. At cathode positions greater than 30 cm, the FWHM becomes difficult to measure, as the discharge-current oscillation peak broadens to a point where the FWHM is on the order of the peak frequency. Even so, the region 1 FWHM is approximately 10 kHz smaller than in region 2 and region 3. Overall, the trend shown in Fig. 7 is that the FWHM increases with cathode radial distance.

C. Radial and Axial Chamber Plates

Similar to the power spectra of the discharge current, an FFT is applied to both the radial plate's collected current and floating-voltage waveforms. Figure 6 shows one representative example of the radial-plate current power spectra and the corresponding discharge-current power spectra. The floating-voltage power spectrum shows a similar peak structure of the current power spectrum, and is not shown. The most notable feature of the radial-plate power-spectrum waveform is the double peak occurring near the discharge-oscillation peak frequency. The discharge-oscillation frequency is 32.2 kHz. In the radial-plate power spectra, there is a spectral peak near the discharge-oscillation frequency at 34.2 kHz and another one at 45 kHz. There is also significant power relative to the noise floor of the power spectra in the sub-10 kHz range. Figure 6 only shows the spectra up to 100 kHz; however, the power spectrum is computed up to the sample rate-limited Shannon–Nyquist frequency of 62.5 MHz. Because of limitations in the 3 dB falloff of the electrical probes, peaks in the radial power spectra above 30 MHz are artifacts. This does not pose an issue for the analysis, as this investigation is

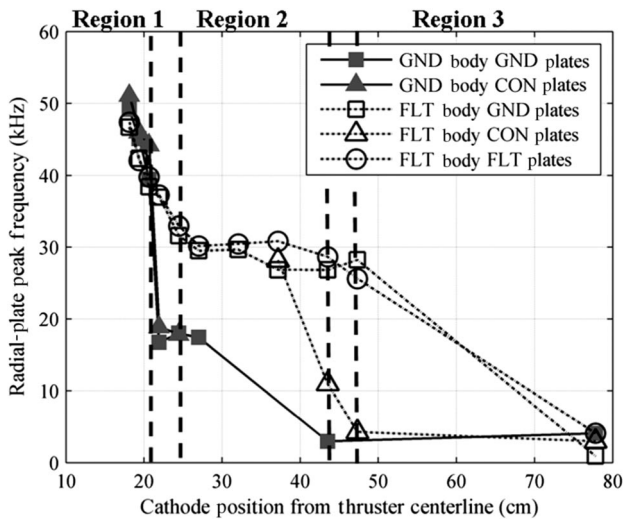


Fig. 8 Peak frequency of the radial-plate current and voltage power spectra as function of cathode position for the thruster-body and plate electrical configurations.

primarily concerned with the plasma phenomenon occurring in the kilohertz range. At frequencies higher than 100 kHz, the power spectra fall off precipitously and indicate the primary energy-containing frequencies are in the sub-100 kHz range. Although Fig. 6 corresponds to one configuration, the multiple-peak nature, the double peak near the discharge-current oscillation is especially prevalent across all thruster configurations where the discharge-current oscillation FWHM is below 10 kHz.

The radial-plate peak frequency has a proportional inverse dependence on cathode position. Figure 8 shows the radial-plate spectral-peak-frequency drop from the 50 kHz range in region 1 to the 5 kHz range in region 3. It is important to note that the region 1 spectral peak frequency is on the order of 50 kHz, but as demonstrated in Fig. 6, the current and voltage radial-plate power spectra have a double-peak structure that includes a lower-frequency spectral peak. The frequency of this secondary peak is on the order of the discharge-current oscillation frequency. In region 2, the radial-plate peak frequencies are of the same order of the discharge-current oscillations. For the floating-body configurations, the region 2 peak frequency is in the 30 kHz range, and for the grounded thruster-body configuration, the region 2 peak frequency is in the 20 kHz range. In region 3, both the thruster-body electrical configurations have peak frequencies in the sub-5 kHz range. Figure 9 shows that the axial-

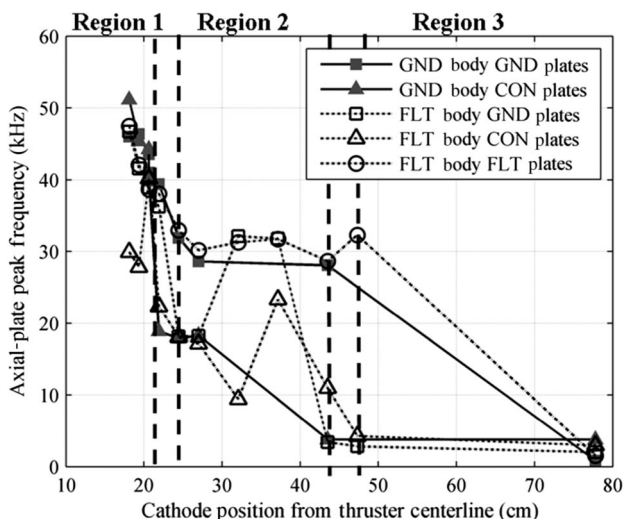


Fig. 9 Peak frequency of the axial-plate current and voltage power spectra as function of cathode position for the thruster-body and plate electrical configurations.

plate peak-frequency cathode-position-dependent behavior exhibits similar peak-frequency characteristics as the discharge current, and confirms previous conclusions drawn by Frieman et al. [13] on the direct coupling of the axial plate to the thruster discharge.

IV. Discussion

The following section explores the connection between the conductive chamber plates and the HET operation through analysis of the time-resolved electrical waveforms captured from voltage and current measurements of the chamber plates and the discharge current. The discussion begins by establishing the connection between the chamber plates and the HET discharge through the use of statistical correlation. After quantifying the statistical correlation between the radial and axial chamber plates and the discharge current, plausible physical mechanisms are identified that could be responsible for the observed correlation. The discussion then moves to an analysis of the physical connection between the chamber plates and the HET discharge, and specifically focuses on the interaction between the radial chamber plate and the HET cathode. The discussion then concludes with a brief overview of the implications on ground testing of HET that are derived from the time-resolved measurements and analysis presented.

A. HET Coupling to the Chamber Plates

Classical statistical correlation is used to assess whether or not the voltage or current waveforms measured from the chamber plates are coupled to the discharge plasma. The correlation coefficient between chamber-plate electrical waveforms and the discharge-current waveform is calculated via MATLAB. The coefficient is calculated via the following equations:

$$\text{cov}(X, Y) = \sum_{i=1}^N \frac{(x_i - \bar{x})(y_i - \bar{y})}{N} \quad (4)$$

$$R(X, Y) = \frac{\text{cov}(X, Y)}{\sqrt{\text{cov}(X, X)\text{cov}(Y, Y)}} \quad (5)$$

in which X , Y , N , cov , and R are the set of numbers representing one waveform, the set of numbers representing the other waveform, the sampling size of the waveform, the covariance between the two waveforms, and the correlation coefficient between waveforms, respectively. The correlation coefficient is a measure of how likely a change in one waveform corresponds to a change in another waveform. For the purposes of this investigation, the distinction between waveforms that are strongly correlated vs waveforms that are weakly correlated is deemed important. A correlation coefficient near unity between two waveforms is classified as strongly correlated, and a correlation coefficient near zero is classified as weakly or not correlated. When analyzing the results of the correlation analysis, changes from strongly correlated to weakly correlated or vice versa correspond to wholesale changes in the nature of the two waveforms being compared. From this perspective, for the purposes of this investigation, small changes, for example, correlation-coefficient changes from 0.95 to 0.91, are not deemed physically significant. To evaluate whether this correlation is attributed to random happenstance and therefore trivial, the P value is also calculated using a standard null-hypothesis test. The P value is a calculation of the percent probability of correlation calculated to be the result of a random sampling of two normal distributions or random processes. Therefore, a lower P value, classically accepted as below 0.05, is indicative of the correlation between two waveforms due to nonrandom processes, and therefore statistically significant.

Figures 10 and 11 show the results of the calculation of the correlation coefficient between the radial-plate electrical waveforms and the discharge current, and the axial-plate electrical waveforms and the discharge current. For all cathode positions, the radial-plate electrical waveform remains strongly negatively correlated to the discharge-current waveform, and the axial-plate electrical waveform

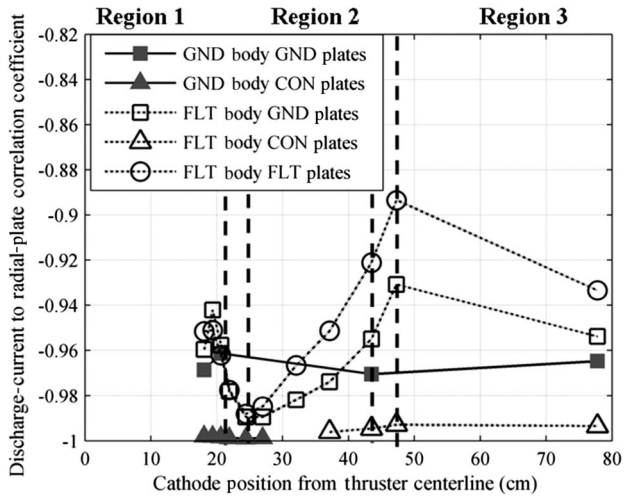


Fig. 10 Radial-plate correlation coefficient as a function of the cathode position for the thruster-body and plate electrical configurations; correlation is taken between the simultaneous waveforms of the discharge current and the radial plate.

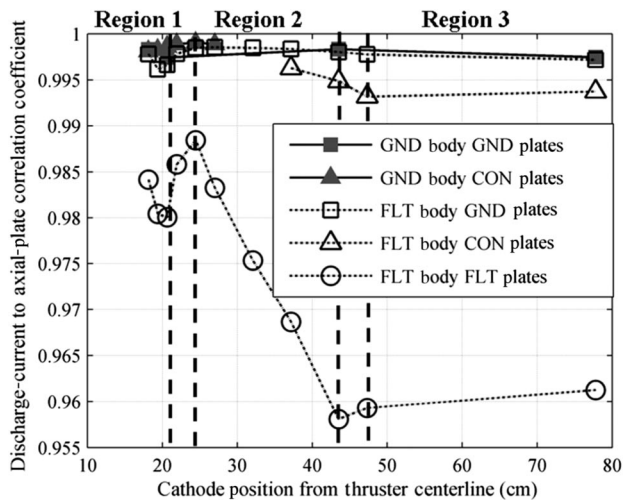


Fig. 11 Axial correlation coefficient as function of the cathode position for the thruster-body and plate electrical configurations; correlation is taken between the simultaneous waveforms of the discharge current and the axial plate.

remains strongly positively correlated to the discharge-current waveform, as shown in Figs. 10 and 11. Because each waveform is composed of 2.5 million data samples, the P value for each of the calculated correlation coefficients is orders of magnitude smaller than the standard 0.05 value for statistical significance. Temporally, the waveform's record length spans 20 ms, which is on the order of 600 fundamental plasma-instability periods estimated with a breathing-mode frequency of 30 kHz. The correlation over such a time frame indicates that the waveforms from the chamber plates and the discharge current are strongly correlated over time, and this correlation is a condition of steady-state HET operation. From a statistical standpoint, the strong temporal correlation and low P value indicate that there is a statistically significant correlation between the electrical waveforms measured from the chamber plates and the discharge-current waveform. Although correlation does not mean causation, such strong statistically significant correlation between the chamber-plate electrical waveforms and the discharge-current waveform merits further investigation to determine if there is a physical mechanism driving this connection.

The quasi-neutral plasma surrounding the axial chamber plate contains both beam ions that originate from the HET discharge and CEX ions. The ions sourced from the HET have a measured downstream energy on the order of 250 V and physically impact the

axial chamber plate [14]. For the floating axial-chamber-plate configuration, the floating voltage is dictated by the balance of ions and electrons collected on the plate (i.e., the local plasma parameters). In all electrical configurations of the axial chamber plate, the electrical waveform measured is governed by the high-energy beam ions sourced from the HET discharge [13]. Time-resolved near-field plume measurements performed by Lobbia [23] show downstream propagation of energetic plasma with a propagation frequency that is closely correlated to the discharge-current oscillation. This energetic plasma propagates downstream of the HET into the chamber. Because the current collection of the axial plate or floating voltage is controlled by the local plasma properties near the axial plate [22], the current collection or floating voltage should fluctuate with changing plasma properties, as the energetic plasma, as described by Lobbia [23], arrives at the axial plate. This process leads to a strong positive correlation between the axial-plate voltage and current waveforms and the HET discharge current, as shown in Fig. 11. Similar physical arguments can be made for the strong correlation between the HET discharge current and radial-plate voltage and current waveform.

In the case of the radial-chamber-plate measurements of current and voltage, the correlation with the discharge-current waveform is still near unity. In contrast to the axial plate, the quasi-neutral plasma surrounding the radial plate is primarily composed of CEX ions and electrons [22]. Therefore, the physical mechanism that governs the interaction between the HET and the radial plate must influence the CEX ions present near the radial plate. It has been demonstrated that the production of the CEX ions is directly linked to the HET discharge and beam [39,40]. Because the production of energetic plasma from the HET discharge occurs with the discharge-current oscillation frequency, the production of CEX ions must also fluctuate with the production of beam ions. Due in part to the CEX ions' thermalized velocity and due in part to the weak positive-ion plasma-potential gradient between the beam to the wall, some of these CEX ions leave the beam and arrive at the radial plate. The presence of these CEX ions is closely tied to the HET discharge, and so it is expected that the local plasma parameters near the radial plate fluctuate with the thruster. Because the current collection and floating voltage of the radial plate are dominated by the fluctuating local plasma conditions, the radial-plate current and voltage waveforms show a strong correlation with the discharge-current waveform. The negative sign of the radial plate to the discharge-current correlation is due to the radial plate collecting a net electron current. This electron current is measured as a negative current. Therefore, an increase in discharge current is accompanied by a larger negative current or negative floating voltage on the radial plate. An example of this behavior is shown in Fig. 12 for a representative section of the radial current and discharge-current waveform used in the correlation analysis.

From the correlation analysis, it is shown that there is a statistically significant and strong correlation between the discharge-current waveform and the chamber-plate current and voltage waveforms. This correlation can be explained through physical processes known to exist in the HET testing environment, and these physical processes have been shown to govern each chamber-plate interaction. Therefore, it can be concluded that the HET discharge current is electrically coupled to the surrounding facility.

B. Electrical Interaction Between the Thruster and the Radial Chamber Plate

1. Evidence of Cathode Coupling to Radial Plate

To aid the discussion of the regional variation in physical mechanisms, it is important to distinguish between two potential sources of electrons collected on the radial plate. The first class of cathode electrons is one in which the electron propagation into the downstream plume is driven by the ions accelerated by the HET discharge. These electrons are pulled into the beam via the electrostatic potential gradient generated by accelerated ions that exit the HET. An example of this electrostatic potential gradient can be seen in Vaudolon et al. [24]. It is through this electrostatic potential

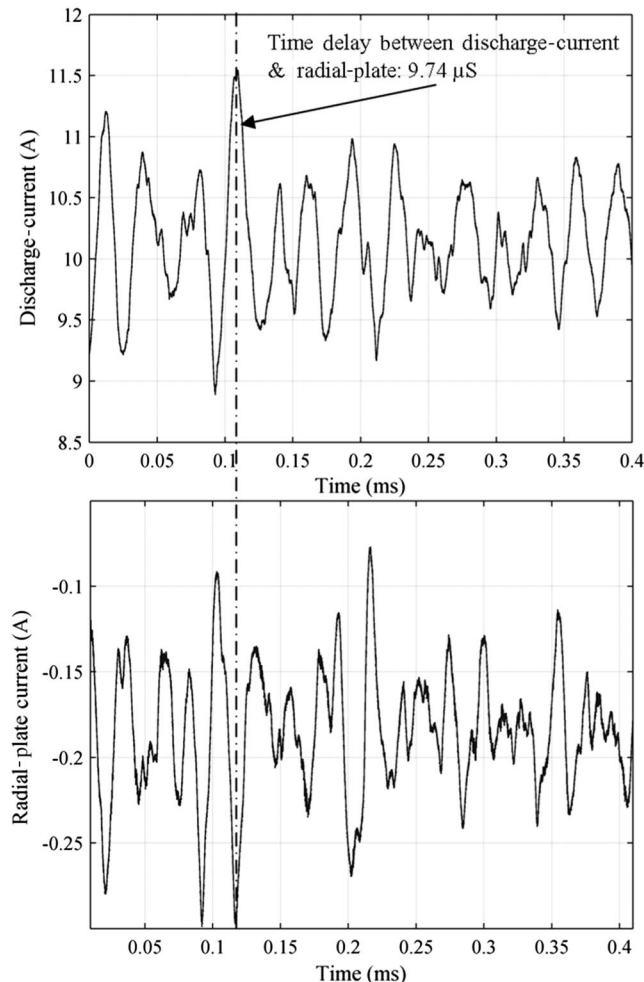


Fig. 12 Raw waveforms measured simultaneously by the oscilloscope; electrical thruster configuration is thruster-body floating, and radial-plate electrical configuration is grounded; figures are offset to accommodate the signal delay as measured by the peak of the cross correlation of the two signals; discharge current (top), radial-plate current to ground (bottom).

gradient that these cathode-sourced electrons, no longer confined by the HET magnetic field, are able to propagate into the downstream plume. Once in the plume, their propagation toward the radial facility walls occurs both thermally and by ambipolar forces pulling electrons along with the CEX ions. These electrons are referred to as “class 1” electrons. The second potential source of electrons incident on the radial plate is one in which the electrons leave the cathode orifice with enough thermal energy that they are unmagnetized by the HET magnetic field. These electrons enter the plume through both the electrostatic potential gradients set up by the accelerated ions and their own thermal velocity. These electrons are affected by ambipolar forces in the plasma, but they also have a strong thermal-velocity component that drives their propagation outward from the cathode orifice. A portion of these electrons has velocity vectors that lead them to impact the radial chamber plate [14]. It is this second class of cathode electrons that is referred to when describing cathode-sourced electrons impacting the radial chamber plate. These electrons are referred to as “class 2” electrons. Both classes of electrons are used for neutralization. The primary difference between the two classes is that the propagation of class 2 electrons to the radial chamber plate is controlled by the electron Hall parameter at the cathode orifice, whereas the propagation of class 1 electrons to the radial plate is controlled by weak plasma-potential gradients and ambipolar forces pulling electrons along with CEX ions into the off-axis region of the plume.

For cathode positions in region 1, cathode electrons are confined by the strong magnetization of the local HET magnetic field, and

thus, the electron-current collection on the radial plate is primarily composed of class 1 electrons. In region 2, the magnetization of cathode electrons is much weaker. Some cathode electrons are confined to the magnetic field, but a large portion of electrons have high-enough thermal energy to escape the HET magnetic field and propagate thermally outward from the cathode orifice. In all cases (region 1, region 2, and region 3), the plasma surrounding the radial plate is dominated by CEX ions. These CEX ions facilitate a transfer of spectral power between the HET discharge and radial plate, as evidenced by the spectral power peaks of the radial-chamber-plate waveform, as seen in Figs. 6 and 8. For cathode positions in region 2, a portion of class 2 (as well as class 1 electrons) high-thermal-energy cathode electrons that are not confined by the HET magnetic field is collected on the radial chamber plate. Evidence of these class 2 electrons impacting the radial chamber plate is seen as elevated spectral power in the sub-5 kHz regime, as shown in Figs. 13 and 14. The actual source of this power in the sub-5 kHz power band can be tied to the cathode as shown in Fig. 14, as spectral power in this frequency range is correspondent to the self-pulsing of the cathode discharge due to the internal plasma resistance of the hollow-cathode discharge [41]. Further evidence indicative that electrons from the cathode directly impinge on the radial plate is shown in Fig. 13. These data were taken from initial thruster testing at a cathode position from a thruster centerline of 18.1 cm. Time-resolved cathode-to-ground voltage measurements did not occur at other cathode positions, and did not occur simultaneously with other data presented thus far. However, this power spectrum shows that the time-resolved cathode-to-ground voltage contains elevated spectra power in the sub-5 kHz range.

For cathode positions in region 3, cathode electrons are no longer magnetized by the HET and thermally propagate outward from the cathode orifice. In comparison to region 2, the flux of class 2 electrons colliding with the radial chamber plate is greater due to lower magnetization and a larger portion of the plume-expansion solid angle intersecting with the radial plate [14]. The rise of the sub-5 kHz spectral power band to the dominant spectral peak, as illustrated in Figs. 8 and 14, indicates that the total flux of electrons impacting the radial plate has a significant population of class 2 electrons. It is important to note that, throughout all regions, the radial-plate electrical-waveform power spectrum has peaks that correspond with the HET discharge-current breathing-mode oscillations. This means the flux of class 2 electrons does not prevent the flux of class 1 electrons onto the radial chamber plate. The regional variation in radial-plate power-spectrum behavior is due to the changing composition of electrons incident on the radial plate. The increases in the sub-5 kHz spectral peak on the radial plate suggest a stronger coupling between the cathode plasma and radial plate. It is unclear, however, if this coupling is a one-way interaction, in which the radial plate does not influence the cathode behavior, or if

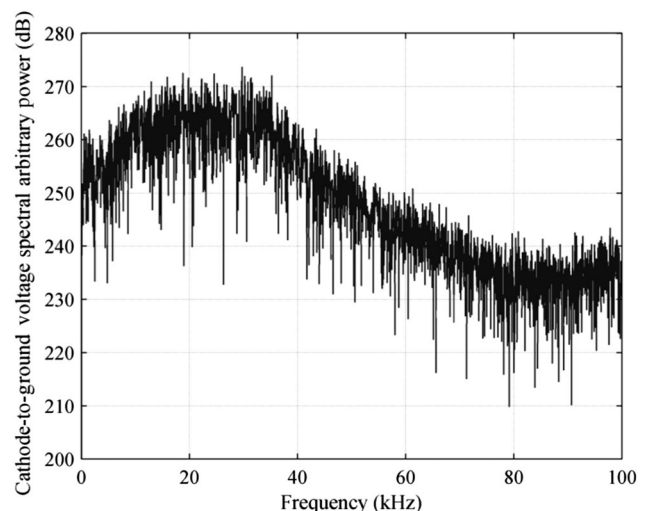


Fig. 13 Representative cathode-to-ground voltage power spectra.

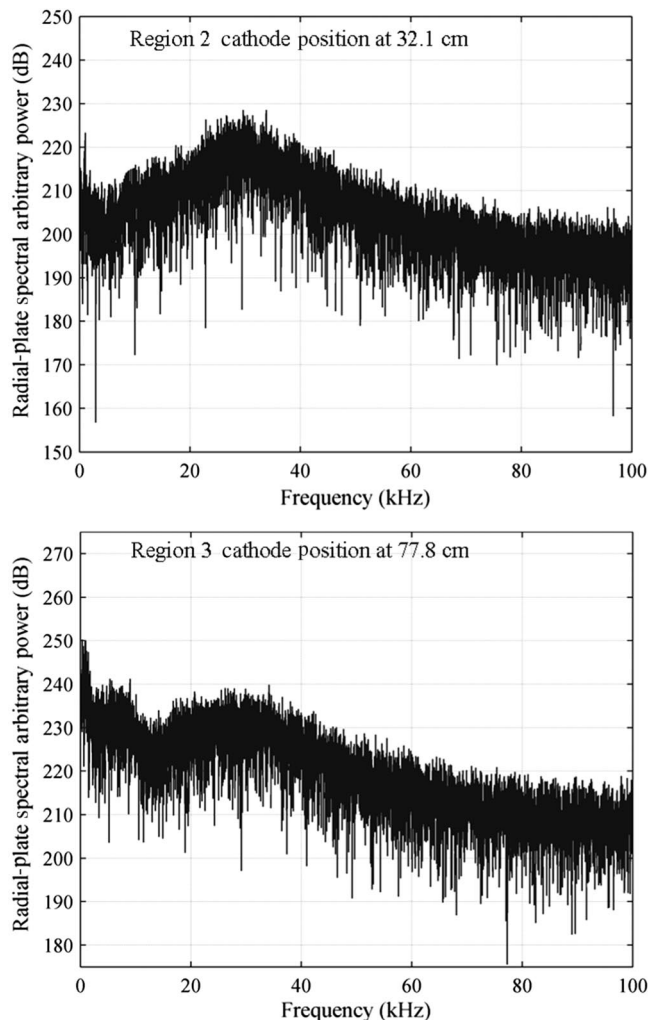


Fig. 14 Radial-plate current-to-ground power spectra for the floating thruster-body electrical configuration; cathode position is at 32.1 cm from thruster centerline (region 2, top); cathode position is at 77.8 cm from thruster centerline (region 3, bottom).

there is feedback from the radial plate that impacts the cathode behavior.

2. Higher-Frequency Spectral Peak of the Radial-Plate Power Spectra

Figure 6 shows the presence of a frequency peak in the 50 kHz range. The two frequency peaks (~ 30 and ~ 50 kHz) of the radial-plate power spectra are found consistently in region 1 and in some cathode positions in region 2. The second higher-frequency peak is at least 1–2 dB stronger than the discharge-oscillation frequency. The source of this power on the radial plate could be from two different sources: self-induced cathode oscillations or a dominant HET plasma oscillatory mode in that frequency range. In the case of the self-induced cathode oscillations, the approximate 50 kHz peak is consistent with cathode measurements taken by Sekerak et al. [20]. However, in region 1 cathode positions, the cathode electrons are confined to the HET magnetic field. Only cathode electrons with the highest energy could propagate toward the facility wall. If it were the case that these high-energy electrons drive the approximate 50 kHz spectral power peak on the radial plate, then it is expected that there should be an increase in power in the 50 kHz range for increasing cathode positions. This is not the case because at large cathode radial positions, the double-peak structure around the discharge oscillation is no longer present in the region 3 radial-plate power spectra. Because the spectral power at the 50 kHz frequency peak is almost equal to the breathing-mode frequency peak, it is more likely that the source of the higher-frequency peak is related to another discharge plasma instability. The data presented in Figs. 6–9 suggest that the

active source of energy for this secondary spectral frequency peak may be due to a plasma-instability mode in the HET discharge. Further investigation in this area is beyond the scope of this paper.

C. HET Discharge-Current Oscillation

From the data presented thus far, there appears to be a connection between the changes in the discharge current and the radial-plate electron current and radial-plate floating voltage. The changes in the peak-to-peak discharge current (Fig. 4), discharge-current peak frequency (Fig. 5), and FWHM of the discharge-current peak frequency (Fig. 7) correspond to a change in the radial-plate peak frequency (Fig. 8) and the radial-plate average collected electron current, as shown by Frieman et al. [14]. Even so, it is unclear as to whether these corresponding changes are due to the increased coupling to the radial plate, due to changes caused by the cathode position relative to the HET magnetic field, or due to both of these aforementioned processes. Much work has been done on cathode position [34–36,42–44], and the general consensus is that the cathode position can be very important in determining the operating behavior of the HET. The actual physical mechanisms that drive this behavior are not fully understood. Work done by Jorns et al. [45] suggests that the formation of ion acoustic turbulence (IAT) is a key physical mechanism in governing electron transport and collisionality in the near cathode-orifice plume. This IAT may be a key physical mechanism that could explain both changes in the radial-plate electron current and the discharge current; however, such data and analysis are beyond the scope of this paper. It is unclear whether the discharge-current behavior relative to the radial plate is due to radial wall coupling or cathode positioning relative to the HET.

D. Impact of the Conductive Wall on HET Operation

The results of the analysis presented in this work indicate that the chamber walls directly influence the plume properties of the HET. As described by Frieman et al. [13,14], the charge-loss rate at the chamber walls can significantly affect the plume plasma potential. The strong temporal statistical correlation between the discharge current, radial plate, and axial plate electrical waveforms indicates that the chamber walls are coupled, in-time, to the HET discharge at all cathode radial positions. The chamber walls represent an artificial electrical boundary condition that forces electron and ion charges to recombine at the wall surface. As evidenced by the strong negative correlation between the discharge current and the radial-chamber-plate current (Fig. 10), increases in the discharge current subsequently result in an increase in the collected electron current. Extending this result to all chamber surfaces, fluctuations caused by the HET in the near-the-chamber-wall local plasma parameters result in changes in the charge-loss rate to the wall. The charge-loss rate to the wall influences the sheath potential drop and can greatly influence the global plasma potential [13,22]. Thus, the chamber wall acts to confine the temporally resolved plasma potential in the plume to within certain bounds. This is not the case in the space environment, where the HET plume electrical boundary condition is not spatially enforced and conductive surfaces that interact with the HET plasma are not held at a constant potential. It has been witnessed from the data and analysis gathered from the Small Missions for Advanced Research in Technology-1 (SMART-1) mission that exposed, low-voltage solar-panel contacts in the HET plume can drive the plasma potential relative to the satellite-bus common and the cathode-to-satellite-bus common voltage in a way that was not anticipated from ground-based testing [46–48]. Such changes in the plasma potential alter the flow of charge particles onto spacecraft surfaces. The changes in cathode-to-satellite-bus common may influence the time-resolved behavior of the HET.

V. Conclusions

It is evident that the cathode position plays a significant role in the discharge-current oscillation frequency, the FWHM of the discharge-current peak frequency, and the peak-to-peak discharge current. These changes in the discharge-current behavior are concurrent with

increases in the collected average electron current on the radial plate and increased power of the sub-5 kHz spectral peaks in the radial-plate power spectrum. Because much work has been done prior to this investigation that shows that the cathode position is critical in determining the HET's overall performance and behavior, it is not yet clear if the observed changes to the discharge are purely due to cathode placement in the magnetic field, purely due to enhanced coupling to the radial plate at larger cathode positions away from the thruster, or due to a mixture of the two aforementioned causes. Because of the observed trends related to the discharge current and the strong statistical correlation between the discharge current and the collected electron current on the radial plate, the results of this work indicate that the radial-plate interaction may be an important influencing factor in the discharge-current characteristics for ground testing. Further examination of the waveforms of the chamber plates revealed that the chamber walls are linked to HET discharge through changes in the plasma potential, and that the chamber walls act in a way to confine the plasma potential to a certain range. Overall, the findings of this investigation suggest that the chamber walls are an important factor to consider when ground testing HETs.

Acknowledgments

Jonathan Walker and Jason Frieman are supported by the National Science Foundation Graduate Research Fellowships under grant number DGE-1148903. The authors would like to thank Sam Langendorf, Natalie Schloeder, and Aaron Schinder for their assistance in the collection of data for and preparation of this paper. The Georgia Institute of Technology would like to acknowledge Lockheed Martin Space Systems Company for their support of this investigation.

References

- [1] Grys, K. D., Mathers, A., Welander, B., and Khayms, V., "Demonstration of 10,400 Hours of Operation on 4.5 kW Qualification Model Hall Thruster," *46th AIAA/ASME/SAE/ASEE Joint Propulsion Conference and Exhibit*, AIAA Paper 2010-6698, July 2010.
- [2] Dankanich, J. W., and McAdams, J., "Interplanetary Electric Propulsion Uranus Mission Trades Supporting the Decadal Survey," *Spaceflight Mechanics 2011, Pts I-III*, Vol. 32, Univelt, San Diego, CA, 2011, pp. 1271-1289.
- [3] Dankanich, J. W., and Oleson, S. R., "Interplanetary Electric Propulsion Chiron Mission Trades Supporting the Decadal Survey," *Spaceflight Mechanics 2011, Pts I-III*, Vol. 32, Univelt, San Diego, CA, 2011, pp. 1245-1255.
- [4] Dumazert, P., and Lagardere-Verdier, S., "PPS 1350 Plasma Thruster Subsystem Life Test," *Third International Conference on Spacecraft Propulsion*, Vol. 465, ESA Publ. Div. C/O Estec, Noordwijk, The Netherlands, 2000, pp. 341-350.
- [5] Walker, M. L. R., "Effects of Facility Backpressure on the Performance and Plume of a Hall Thruster," Ph.D. Thesis, Aerospace Engineering, Univ. of Michigan, Ann Arbor, MI, 2005, p. 254.
- [6] Brown, D. L., and Gallimore, A. D., "Evaluation of Facility Effects on Ion Migration in a Hall Thruster Plume," *Journal of Propulsion and Power*, Vol. 27, No. 1, 2011, pp. 573-585. doi:10.2514/1.b34068
- [7] Azziz, Y., Martinez-Sanchez, M., and Szabo, J., "Determination of In-Orbit Plume Characteristics from Laboratory Measurements," *42nd AIAA/ASME/SAE/ASEE Joint Propulsion Conference and Exhibit*, AIAA Paper 2006-4484, July 2006.
- [8] Diamant, K. D., Liang, R., and Corey, R. L., "The Effect of Background Pressure on SPT-100 Hall Thruster Performance," *50th AIAA/ASME/SAE/ASEE Joint Propulsion Conference*, AIAA Paper 2014-3710, July 2014.
- [9] Huang, W., Kamhawi, H., Lobbia, R. B., and Brown, D. L., "Effect of Background Pressure on the Plasma Oscillation Characteristics of the HiVHAC Hall Thruster," *50th AIAA/ASME/SAE/ASEE Joint Propulsion Conference*, AIAA Paper 2014-3708, July 2014.
- [10] Kamhawi, H., Huang, W., Haag, T., and Spektor, R., "Investigation of the Effects of Facility Background Pressure on the Performance and Operation of the High Voltage Hall Accelerator," *50th AIAA/ASME/SAE/ASEE Joint Propulsion Conference*, AIAA Paper 2014-3707, July 2014.
- [11] Nakles, M. R., and Hargus, W. A., Jr., "Background Pressure Effects on Ion Velocity Distribution Within a Medium-Power Hall Thruster," *Journal of Propulsion and Power*, Vol. 27, No. 4, 2011, pp. 737-743. doi:10.2514/1.48027
- [12] Walker, M. L. R., Victor, A. L., Hofer, R. R., and Gallimore, A. D., "Effect of Backpressure on Ion Current Density Measurements in Hall Thruster Plumes," *Journal of Propulsion and Power*, Vol. 21, No. 1, 2005, pp. 408-415. doi:10.2514/1.7713
- [13] Frieman, J. D., King, S. T., Walker, M. L. R., Khayms, V., and King, D., "Role of a Conducting Vacuum Chamber in the Hall Effect Thruster Electrical Circuit," *Journal of Propulsion and Power*, Vol. 30, No. 6, 2014, pp. 1471-1479. doi:10.2514/1.B35308
- [14] Frieman, J. D., Walker, J. A., Walker, M. L. R., Khayms, V., and King, D., "Electrical Facility Effects on Hall Effect Thruster Cathode Coupling: Performance and Plume Properties," *Journal of Propulsion and Power*, 2015, pp. 1-14. doi:10.2514/1.B35683
- [15] Walker, J. A., Frieman, J. D., Walker, M. L., Khayms, V., King, D., and Peterson, P., "Electrical Facility Effects on Hall Effect Thruster Cathode Coupling: Discharge Oscillations and Facility Coupling," *50th AIAA/ASME/SAE/ASEE Joint Propulsion Conference*, AIAA Paper 2014-3711, July 2014.
- [16] Chouei, E. Y., "Plasma Oscillations in Hall Thrusters," *Physics of Plasmas*, Vol. 8, No. 4, 2001, pp. 1411-1426. doi:10.1063/1.1354644
- [17] Hara, K., Sekerak, M. J., Boyd, I. D., and Gallimore, A. D., "Perturbation Analysis of Ionization Oscillations in Hall Effect Thrusters," *Physics of Plasmas*, Vol. 21, No. 12, 2014, Paper 122103 doi:10.1063/1.4903843
- [18] McDonald, M. S., Sekerak, M. J., Gallimore, A. D., and Hofer, R. R., "Plasma Oscillation Effects on Nested Hall Thruster Operation and Stability," *2013 IEEE Aerospace Conference*, IEEEAC Paper #2502, March 2013.
- [19] Sekerak, M., "Plasma Oscillations and Operational Modes in Hall Effect Thrusters," Ph.D. Thesis, Aerospace Engineering, Univ. of Michigan, Ann Arbor, MI, 2014, p. 280.
- [20] Sekerak, M., Longmeir, B., Gallimore, A., Huang, W., Kamhawi, H., Hofer, R. R., Jorns, B., and Polk, J. E., "Mode Transitions in Magnetically Shielded Hall Effect Thrusters," *50th AIAA/ASME/SAE/ASEE Joint Propulsion Conference*, AIAA Paper 2014-3511, July 2014.
- [21] Sekerak, M., McDonald, M., Hofer, R., and Gallimore, A., "Hall Thruster Plume Measurements from High-Speed Dual Langmuir Probes with Ion Saturation Reference," *2013 IEEE Aerospace Conference*, March 2013.
- [22] Goebel, D. M., and Katz, I., *Fundamentals of Electric Propulsion: Ion and Hall Thrusters*, Wiley, Hoboken, NJ, 2008, pp. 37-86, 376-379, 393-421.
- [23] Lobbia, R. B., "A Time-Resolved Investigation of the Hall Thruster Breathing Mode," *Aerospace Engineering*, Univ. of Michigan, Ann Arbor, MI, 2010, p. 179.
- [24] Vaudolon, J., Khiar, B., and Mazouffre, S., "Time Evolution of the Electric Field in a Hall Thruster," *Plasma Sources Science and Technology*, Vol. 23, No. 2, 2014, pp. 1-6. doi:10.1088/0963-0252/23/2/022002
- [25] Hara, K., Sekerak, M. J., Boyd, I. D., and Gallimore, A. D., "Mode Transition of a Hall Thruster Discharge Plasma," *Journal of Applied Physics*, Vol. 115, No. 20, 2014, Paper 203304. doi:10.1063/1.4879896
- [26] Ermilov, A. N., Eroshenkov, V. F., Novichkov, D. N., Kovalenko, Y. A., Saponova, T. M., Chernyshev, T. V., and Shumilin, A. P., "Oscillations of the Hall Current in a Hall Thruster with an Anode Layer," *High Temperature*, Vol. 52, No. 1, 2014, pp. 360-365. doi:10.1134/s0018151x14030109
- [27] Raitses, Y., Griswold, M., Ellison, L., Parker, J., and Fisch, N., "Studies of Rotating Spoke Oscillations in Cylindrical Hall Thrusters," *48th AIAA/ASME/SAE/ASEE Joint Propulsion Conference and Exhibit*, AIAA Paper 2012-4179, July 2012.
- [28] Ellison, C. L., Raitses, Y., and Fisch, N. J., "Fast Camera Imaging of Hall Thruster Ignition," *IEEE Transactions on Plasma Science*, Vol. 39, No. 11, 2011, pp. 2950-2951. doi:10.1109/tps.2011.2121925
- [29] Kieckhafer, A., and Walker, M. L. R., "Recirculating Liquid Nitrogen System for Operation of Cryogenic Pumps," *32nd International Electric Propulsion Conference*, IEPC Paper 2011-217, Sept. 2011.
- [30] Tilford, C. R., "Sensitivity of Hot Cathode Ionization Gages," *Journal of Vacuum Science & Technology A*, Vol. 3, No. 1, 1985, pp. 546-550. doi:10.1116/1.572991
- [31] Walker, M. L. R., and Gallimore, A. D., "Neutral Density Map of Hall Thruster Plume Expansion in a Vacuum Chamber," *Review of Scientific*

- Instruments*, Vol. 76, No. 5, 2005, Paper 053509.
doi:10.1063/1.1915011
- [32] "571 Ionization Gauge Tube Instruction Manual," Manual No. 6999905571 Revision C, 2002.
- [33] McLean, C., McVey, J., and Schappell, T., "Testing of a U.S.-Built HET System for Orbit Transfer Applications," *35th Joint Propulsion Conference and Exhibit*, AIAA Paper A99-31318, June 1999.
- [34] Sommerville, J. D., and King, L., "Effect of Cathode Position on Hall-Effect Thruster Performance and Near-Field Plume Properties," *44th AIAA/ASME/SAE/ASEE Joint Propulsion Conference and Exhibit*, AIAA Paper 2007-5174, 2008.
- [35] Sommerville, J. D., and King, L. B., "Hall-Effect Thruster-Cathode Coupling, Part I: Efficiency Improvements from an Extended Outer Pole," *Journal of Propulsion and Power*, Vol. 27, No. 4, 2011, pp. 744–753. doi:10.2514/1.50123
- [36] Sommerville, J. D., and King, L. B., "Hall-Effect Thruster-Cathode Coupling, Part II: Ion Beam and Near-Field Plume," *Journal of Propulsion and Power*, Vol. 27, No. 4, 2011, pp. 754–767. doi:10.2514/1.50124
- [37] Spektor, R., Willhoff, M. A., Beiting, E., and Diamant, K., "Characterization of the High Power Propulsion System Subscale," *60th JANNAF Propulsion Meeting*, JANNAF Paper 2013-3142, April 2013.
- [38] Hofer, R. R., and Anderson, J. R., "Finite Pressure Effects in Magnetically Shielded Hall Thrusters," *50th AIAA/ASME/SAE/ASEE Joint Propulsion Conference*, AIAA Paper 2014-3709, July 2014.
- [39] Boyd, I. D., and Dressler, R. A., "Far Field Modeling of the Plasma Plume of a Hall Thruster," *Journal of Applied Physics*, Vol. 92, No. 4, 2002, pp. 1764–1774. doi:10.1063/1.1492014
- [40] King, L. B., "Transport-Property and Mass Spectral Measurements in the Plasma Exhaust Plume of a Hall-Effect Space Propulsion System," *Aerospace Engineering*, Univ. of Michigan, Ann Arbor, MI, 1998.
- [41] Qin, Y., He, F., Jiang, X. X., Xie, K., and Ouyang, J. T., "Self-Pulsing of Hollow Cathode Discharge in Various Gases," *Physics of Plasmas*, Vol. 21, No. 7, 2014, Paper 073501. doi:10.1063/1.4885640
- [42] Hofer, R., Johnson, L., Goebel, D., and Fitzgerald, D., "Effects of an Internally-Mounted Cathode on Hall Thruster Plume Properties," *42nd AIAA/ASME/SAE/ASEE Joint Propulsion Conference and Exhibit*, AIAA Paper 2006-4482, July 2006.
- [43] Walker, M. L. R., and Gallimore, A. D., "Hall Thruster Cluster Operation with a Shared Cathode," *Journal of Propulsion and Power*, Vol. 23, No. 1, 2007, pp. 528–536. doi:10.2514/1.23688
- [44] Hofer, R. R., Johnson, L. K., Goebel, D. M., and Wirz, R. E., "Effects of Internally Mounted Cathodes on Hall Thruster Plasma Properties," *IEEE Transactions on Plasma Science*, Vol. 36, No. 5, 2008, pp. 2004–2014. doi:10.1109/tps.2008.2000962
- [45] Jorns, B. A., Mikellides, I. G., and Goebel, D. M., "Ion Acoustic Turbulence in a 100-A LaB6 Hollow Cathode," *Physical Review E*, Vol. 90, No. 6, 2014, Paper 063106. doi:10.1103/PhysRevE.90.063106
- [46] Passaro, A., Vicini, A., Nania, F., and Biagioni, L., "Numerical Rebuilding of SMART-1 Hall Effect Thruster Plasma Plume," *Journal of Propulsion and Power*, Vol. 26, No. 1, 2010, pp. 149–158. doi:10.2514/1.36921
- [47] Koppel, C., Marchandise, F., Prioul, M., Estublier, D., and Darnon, F., "The Smart-1 Electric Propulsion Subsystem Around the Moon: In Flight Experience," *41st AIAA/ASME/SAE/ASEE Joint Propulsion Conference and Exhibit*, AIAA Paper 2005-3671, July 2005.
- [48] Koppel, C., Marchandise, F., Estublier, D., and Jolivet, L., "The Smart-1 Electric Propulsion Subsystem In Flight Experience," *40th AIAA/ASME/SAE/ASEE Joint Propulsion Conference and Exhibit*, AIAA Paper 2004-3435, July 2004.

J. Blandino
Associate Editor